# Fire-Resistant Wall-Climbing UAV for Victim Detection in Urban Search and Rescue Missions

Vedant Hambire\*, Harsh Yadav, Dipshikha Hazari and Satyam Singh National Institute of Technology, Agartala, India

Keywords: Wall-Climbing UAV, Fireproof Drone, Urban Search and Rescue (USAR), YOLOv8, Optical Flow,

MediaPipe, Tilt-Rotor Mechanism, CFD, FEA, ROS, Alive Human Detection.

Abstract: Unmanned Aerial Vehicles (UAVs) have become invaluable in high-stakes search and rescue operations in

fire-prone and fire-damaged environments due to their capabilities in victim locating and situation analysis. This paper describes the design, simulation, and realization of a fire-resistant, wall-climbing UAV with a human alive detection system powered by AI. The UAV includes a custom-designed H-frame made out of PLA which is thrust vectoring EDFs attached to a tilt-rotor system permitting vertical hovering and traversing. Structural and aerodynamic aspects were verified with FEA and CFD simulations performed on SimScale. To allow for autonomous victim detection, the UAV system includes a real-time human detector based on YOLOv8 with and optical flow and MediaPipe-based eye tracking to classify people as conscious, unconscious, dead, or blocked out. The UAV's mission computer, which comprises a Raspberry Pi with ROS, records would-detect status and location, and outputs tagged geo-coordinates for mission planning in real-time. Simulation and ground testing would confirm the system's viability in heat-intensive, debris-laden environments, advancing the development of autonomous aerial platforms for disaster response, firefighting,

environments, advancing the development of autonomous aerial platforms for disaster response, fi and urban search and rescue (USAR) operations.

## 1 INTRODUCTION

Unmanned Aerial Vehicles (UAVs) have emerged as crucial instruments in a variety of fields over the past ten years, such as search and rescue, surveillance, and disaster response (Mulgaonkar et al., 2016), (Dudek & Jenkin, 2010). UAVs that can withstand high-risk situations like industrial settings, collapsed structures, and fire-prone areas are becoming more and more necessary for these applications.

Despite their proficiency in aerial reconnaissance, traditional multirotor platforms are constrained by their poor wall traversal capabilities, heat sensitivity, and incapacity to identify incapacitated victims (Murphy, 2004). Researchers have developed fireproof UAVs with thermal insulation layers, such as Nomex, ceramic coatings, or silica aerogels, to get around these limitations. These layers protect electronic systems from high ambient temperatures (Zhang et al., 2021), (Lee et al., 2020), (Tan et al., 2021). Wall-climbing UAVs that draw inspiration from biological systems like geckos, insects, and bats have been developed as a result of parallel

developments in surface adhesion and locomotion (Kim et al., 2018), (Li et al., 2017). These systems scale vertical or inverted surfaces using suction mechanisms (Sun et al., 2021), electro-adhesion (Spenko et al., 2012), or magnet-based gripping (Wang et al., 2021). Most are less effective in multihazard environments because they lack integration with fire survivability or robust perception systems, despite being effective in confined spaces.

UAVs can now accurately identify human targets on their own thanks to recent advancements in real-time computer vision, especially in object detection using deep learning models like YOLO (You Only Look Once) (Redmon et al., 2018). But YOLO by itself is unable to distinguish between people who are conscious, unconscious, or deceased. In order to close this gap, scientists have integrated optical flow to identify subtle thoracic movements that are suggestive of breathing (Akhloufi et al., 2020), (Sharma & Mahapatra, 2021). In our work, we evaluate breathing using the Farneback method on grayscale frame differences, which enables the system to classify victims into subtle states.

<sup>\*</sup> Corresponding author: vedanthambire 568@email.com

We use MediaPipe FaceMesh, a landmark detection framework created by Google, to further evaluate consciousness. This framework allows for accurate measurement of Eye Aspect Ratio (EAR), which infers blink rates and eye closure (Zhang et al., 2020). A complete "alive detection" pipeline that can classify data in real time into four different states— Alive & Conscious, Alive but Unconscious, Dead, and Obstructed/Not Visible—is made possible by the combination of YOLOv8, optical flow, and MediaPipe. This system would be powered by a small Raspberry Pi 4B onboard computer that runs ROS and connects via MAVLink to a flight controller that is compatible with Pixhawk. The UAV would be equipped with an MTF-01P optical flow sensor for indoor navigation and Intel RealSense cameras for depth and odometry, making it ready for both controlled and unpredictably changing conditions.

To ensure stable control during wall contact, transition, and flight, we would implement a Model Predictive Control (MPC) architecture. This control strategy adapts across three behavioural modes—sticking, tilting, and climbing—with specific optimisations for wheel torque, gear actuation, and thrust modulation. The UAV's dynamic model is simulated using ROS2 and Gazebo, ensuring that the control algorithm respects physical constraints and delivers energy-efficient performance.

Our work therefore unifies fireproofing, surface adhesion, advanced vision-based perception, and predictive control into a single hybrid UAV platform, addressing multiple gaps in current USAR (Urban Search and Rescue) technologies. The integration of resilient materials, sensor-rich electronics, and deep learning allows this system to operate autonomously in highly dynamic and hazardous environments.

## 2 DESIGN STRATEGY

The proposed UAV is inspired by the tilt-rotor wall-climbing concept introduced by Myeong and Myung (Myeong & Myung, 2020), where thrust vectoring and surface traction enable stable vertical attachment. This design incorporates fire-resistant structural elements and an AI-based alive detection system tailored for disaster zones. The UAV uses a modified H-frame made of PLA and carbon fibre rods for optimal strength-to-weight performance. Developed in SolidWorks and analysed in ANSYS, the frame withstands perching and wall-impact loads. Four EDFs (two front, two rear) are mounted on servo-

actuated tilting arms, enabling transitions between horizontal flight and vertical climbing. MG995 servos drive a 1:1 gear system for smooth tilt control, with a selected angle of 59.2° optimised for wall adhesion (friction coefficient = 0.5). Passive wheels assist vertical mobility post-attachment. CFD simulations in SimScale confirm stable aerodynamics near walls; FEA validates joint and strut integrity. For victim detection, a Raspberry Pi runs YOLOv8 with optical analysis to monitor thoracic motion, distinguishing live victims. On detection, GPS coordinates are transmitted to responders. This builds on approaches by Patel et al. (Patel et al., 2020) and Li et al. (Li et al., 2021), highlighting deep learning's role in disaster-zone reconnaissance. Upon detection, the drone transmits GPS coordinates to responders. This builds on approaches by Patel et al. (Patel et al., 2020) and Li et al. (Li et al., 2021), who demonstrated deep learning's value in disaster-zone reconnaissance.



Figure 1: Final SolidWorks model of the wall-climbing UAV; isometric view of the UAV showing the tilt-rotor H-frame layout with EDFs and passive wall-contact wheels; Front view illustrating vertical alignment of ducted fans and the symmetric gear-driven shaft for tilt control.

#### 2.1 Drone Frame

The UAV uses a compact H-frame designed in SolidWorks, optimised for structural rigidity and balanced load distribution. The main frame is 3D printed in PLA and laterally reinforced with carbon fibre rods supporting the rotating EDF modules. A 165 mm-wide central platform includes precise cutouts for mounting the servo-tilt system, NxtPX4V2 flight controller (sandwiched for vibration damping), Raspberry Pi, battery, and passive wheels aiding wall climbing and stability.

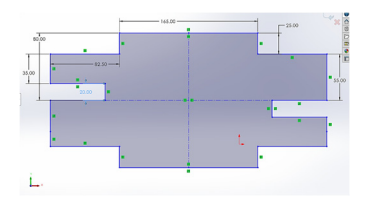




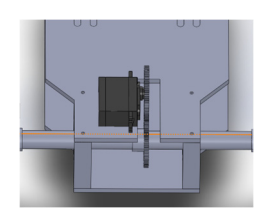
Figure 2: SolidWorks sketch of the PLA frame with key dimensions and cut-outs for mounting components. Top view of the UAV assembly showing component placement and symmetric EDF-wheel layout.

#### 2.2 Tilt Rotor Mechanism

The UAV employs four EDF motors (two front, two rear) housed in custom PLA cases that function as both enclosures and supports for the wall-climbing mechanism. These cases are mounted on a 16 mm carbon fibre shaft driven by a 1:1 spur gear system coupled to an MG995 high-torque servo, enabling symmetric tilting of the EDFs. Following the tilt-rotor approach of Myeong and Myung (Myeong & Myung, 2020), this design allows smooth transitions between horizontal flight and wall adhesion. Each EDF case also integrates a secondary mount for wall-contact wheels, redesigned with ball bearings for low-friction movement along vertical surfaces. The wheels, fabricated from ABS for impact resistance and low weight, support wall climbing, while the required tilt angle  $(\theta)$  is determined using equation (1).

$$\tan(\theta) = mg/\mu T \tag{1}$$

Where m is UAV mass, g is gravity, T is thrust per motor, and  $\mu$  is the friction coefficient. For a UAV mass of 2 kg, EDF thrust of 1.25 kgf per unit, and  $\mu$  = 0.5, the calculated optimal tilt angle is approximately 59.2°, aligning with the previous research findings (Myeong & Myung, 2020). This mechanism allows the UAV to redirect thrust perpendicularly during perching and revert for free flight, enabling hybrid aerial-wall locomotion.



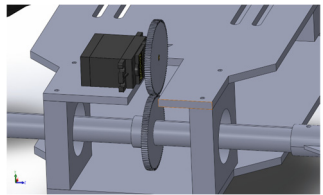


Figure 3: Top view of the servo-driven spur gear mechanism enabling symmetric EDF tilt via a carbon fibre shaft. Isometric view of the tilt-rotor gear assembly integrated into the UAV frame.

#### 2.3 Electronics

The UAV is equipped with electronics tailored for high-thrust propulsion, autonomous wall-climbing, and onboard human detection. At its core is the NxtPX4V2 flight controller, handling motor control, sensor fusion, and stabilisation. Propulsion is delivered via four Powerfun 70 mm EDF motors (2.2 kgf thrust each), driven by a Hobbywing XRotor G2 4-in-1 65A ESC with 6S input and DShot1200 protocol for low-latency response. A Pro-Range 13000mAh 6S 25C LiPo battery (1.56 kg) powers the system, offering ~8.5 minutes of flight and a 1.67 thrust-to-weight ratio, enabling stable lift and climbing. Power is split via XT90 connectors, with two UBECs (5V and 12V) providing isolated supply to MG995 servos (for tilt-rotor actuation) and the onboard compute unit.

Flight Time (minutes) =  $(C \times V \times \eta / P) \times 60$ 

Using the values:

(Battery Capacity) C = 13 Ah, (Battery Voltage) V = 22.2 V, (Discharge Efficiency)  $\eta = 0.85$ , (Average Power Consumption) P = 1450 W

Flight Time  $\approx 8.5$  minutes

This estimated value is based on moderate hover and cruise conditions. Final validation will be done using telemetry logs and stopwatch measurements during prototype testing. For perception and positioning, the UAV uses the MTF-01P optical flow and range sensor, NEO-M8N GPS with compass, and SiK Telemetry Radio V3 for long-range communication. Two Intel RealSense cameras D435i (depth) and T265 (odometry) enable indoor navigation and visual detection. These feed into a Raspberry Pi 4B running ROS for onboard AI inference, including a YOLOv5tiny model for real-time human detection and optical flow-based breathing analysis. The Pi communicates with the flight controller via MAVLink for decisionmaking. The system is manually operable through a TX16S Mark II radio with fail-safe support via SiK link.

To meet power and endurance requirements within a 1.5 kg battery limit, a Tattu 6S 12000 mAh 25C LiPo battery was selected. Delivering 22.2 V nominal voltage and up to 300 A continuous discharge, it comfortably supports the combined 260 A draw of four EDFs rated at 65 A each. Weighing ~1.43 kg, the battery keeps the UAV's allup weight (AUW) at 4.5 kg, as confirmed by the integrated mass breakdown. Flight time is estimated at ~8.5 minutes under high-load conditions. The four

EDFs generate a total of 8.8 kgf static thrust. At a  $60^{\circ}$  tilt, the vertical thrust component reaches ~7.5 kg, yielding a thrust-to-weight ratio of 1.67, which ensures stable vertical lift and wall-climbing. The horizontal thrust (~4.6 kg) supports wall traction and transition control.

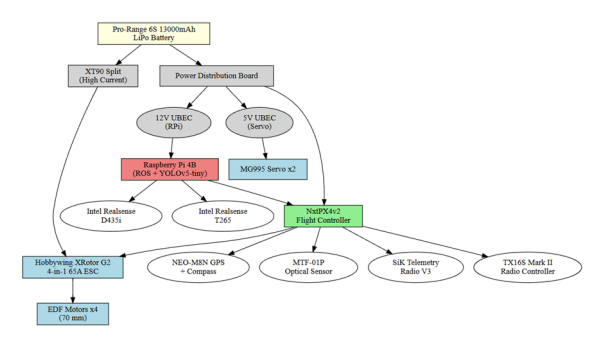


Figure 4: Power and control architecture of the UAV, illustrating the integration of the propulsion, perception, computation, and communication subsystems

## 2.4 Fireproofing

To enhance survivability in fire-prone environments, the UAV's base frame is 3D printed in lightweight PLA, ideal for rapid prototyping. However, due to PLA's low thermal resistance (~60 °C), it is coated with Nomex a flame-retardant aramid fibre known for high thermal stability and low weight. Widely used in aerospace and firefighting gear, Nomex withstands temperatures up to 370 °C without melting or dripping, while maintaining structural integrity. With a density of just 1.38 g/cm³, it adds minimal weight to the drone.

#### 2.5 Mathematical Model

The system is defined using three coordinate frames: the world frame, body frame, and individual rotor frames. The world frame (Xw, Yw, Zw) is a fixed inertial reference, while the body frame (Xb, Yb, Zb) is centered at the UAV's center of gravity and used for dynamic modelling and control. Each rotor (R1–R4) has a local frame initially aligned with the body frame but can rotate around the yaw axis and tilt as actuated. The UAV uses four Electric Ducted Fan (EDF) rotors, each capable of dual-axis tilting (pitch and roll). Two servomotors per side enable paired tilting: R1 with R4, and R2 with R3.

Thrust Vector in Rotor Frame

$$\vec{T}_r = \begin{bmatrix} 0 \\ 0 \\ T \end{bmatrix}$$
 (Thrust acts along the rotor's local Z-axis)

Rotation Due to Dual-Axis Tilt

$$R_{\text{tilt}} = R_{\chi}(\alpha) \cdot R_{y}(\beta)$$

$$R_{\chi}(\alpha) = \begin{bmatrix} 1 & 0 & 0 \\ 0 & \cos \alpha & -\sin \alpha \\ 0 & \sin \alpha & \cos \alpha \end{bmatrix}$$

$$R_{y}(\beta) = \begin{bmatrix} \cos \beta & 0 & \sin \beta \\ 0 & 1 & 0 \\ -\sin \beta & 0 & \cos \beta \end{bmatrix}$$

$$\vec{T}_{\text{tilted}} = R_{\chi}(\alpha) \cdot R_{\gamma}(\beta) \cdot \vec{T}_{r}$$

Rotor Orientation w.r.t. Body Frame (Yaw Offset):

$$R_z(\psi_i) = \begin{bmatrix} \cos \psi_i & -\sin \psi_i & 0\\ \sin \psi_i & \cos \psi_i & 0\\ 0 & 0 & 1 \end{bmatrix}$$

Thrust in Body Frame:

$$\vec{T}_{\text{body}} = R_z(\psi_i) \cdot R_x(\alpha) \cdot R_y(\beta) \cdot \begin{bmatrix} 0 \\ 0 \\ T \end{bmatrix}$$

UAV Orientation in World Frame (Euler ZYX)

$$R_{\text{world}}^{\text{body}} = R_z(\psi) \cdot R_y(\theta) \cdot R_x(\phi)$$

The rotation matrix from the body frame to the world frame using the ZYX Euler angle convention (yaw  $\psi$ , pitch  $\theta$ , roll  $\phi$ ) is given by:

$$R_{\text{world}}^{\text{body}} = R_z(\psi) \cdot R_y(\theta) \cdot R_x(\phi)$$

$$R = \begin{bmatrix} c_\psi c_\theta & c_\psi s_\theta s_\phi - s_\psi c_\phi & c_\psi s_\theta c_\phi + s_\psi s_\phi \\ s_\psi c_\theta & s_\psi s_\theta s_\phi + c_\psi c_\phi & s_\psi s_\theta c_\phi - c_\psi s_\phi \\ -s_\theta & c_\theta s_\phi \end{bmatrix}$$



Figure 5: Reference frames of the UAV. The world frame (Xw,Yw,Zw) is a fixed inertial frame. The body frame (Xb,Yb,Zb) is attached to the UAV's center of gravity (CG).

Final Thrust Vector in World Frame is:

$$\begin{split} \vec{T}_{\text{world}} &= R_{\text{world}}^{\text{body}} \cdot \vec{T}_{\text{body}} \\ \vec{T}_{\text{world}} &= R_z(\psi) \cdot R_y(\theta) \cdot R_x(\phi) \cdot R_z(\psi_i) \cdot R_x(\alpha) \cdot R_y(\beta) \cdot \begin{bmatrix} 0 \\ 0 \\ T \end{bmatrix} \end{split}$$

Where:

 $\psi_i$ : Yaw position of the rotor relative to the UAV body,  $\alpha, \beta$ : Rotor tilt angles (dual-axis), T: Thrust magnitude (in rotor frame)

#### 3 ANALYSIS

To ensure structural robustness, aerodynamic efficiency, and fire resilience, the UAV was simulated using SimScale. The frame was modelled with Polylactic Acid (PLA), while 16 mm carbon fibre rods reinforced the tilt mechanism and motor shafts. Structural integrity was assessed via Finite Element Analysis (FEA) to identify stress concentrations under load. Computational Fluid Dynamics (CFD) simulations examined airflow during flight and wall climbing. The results informed key design choices.

# 3.1 Frame Analysis

To evaluate the structural integrity of the UAV frame under operational loading conditions, a static structural analysis was performed using the Finite Element Analysis (FEA) module in SimScale. The frame model, derived from the SolidWorks assembly, consists of PLA. A fine mesh was applied with maximum edge length of 0.005 m and minimum of 0.001 m, generating approximately 944,000 nodes for accurate stress resolution.

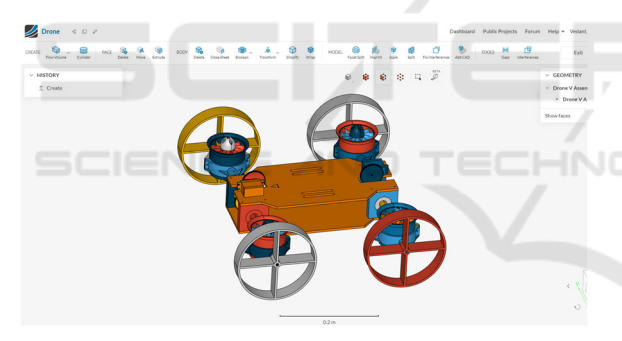


Figure 6: Meshing setup for structural FEA in SimScale.

The material properties used for PLA were: Young's Modulus of 3.5 GPa, Poisson's ratio of 0.36, and density of 1.24 g/cm³, while carbon fibre rods were assumed to be rigid due to their high stiffness. Boundary conditions included fixed supports at the motor mount joints and load application points corresponding to the EDF thrust force. A gravity vector of 9.81 m/s² was applied globally to simulate self-weight. Contacts between components were defined as bonded, and the analysis assumes linear elastic behavior with no material plasticity.

The simulation results revealed that the maximum von Mises stress occurred at the junctions of the carbon fibre rods and the PLA plates, especially around the motor mount zones, with a peak stress of approximately 48.3 MPa, which is well below PLA's

typical yield strength (~60 MPa), ensuring a safe stress margin. The displacement contour showed a maximum deflection of around 1.83 mm. The Cauchy stress distribution confirmed that stresses were concentrated around bolt holes and load-bearing corners, validating the structural importance of reinforcement via carbon fibre rods. The factor of safety was maintained above 1.25 throughout critical regions.

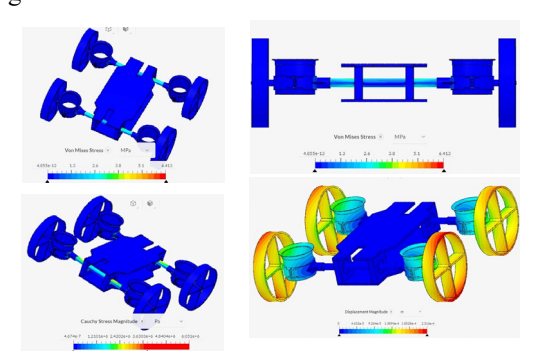


Figure 7: FEA results showing von Mises stress distribution, stress concentration near carbon fibre shafts, Cauchy stress zones around load paths, and total displacement.

# 3.2 CFD Analysis

To assess the aerodynamic performance of the UAV during both horizontal flight and inclined wall-climbing phases, a steady-state incompressible turbulent flow simulation was performed using the k-omega SST model in SimScale. An inlet velocity of 15 m/s was specified at the front face, while the outlet was set to zero relative pressure, replicating realistic cruise conditions. All solid surfaces were treated as no-slip walls, and the far-field boundaries were defined with slip conditions. The mesh comprised over 3.2 million cells, ensuring sufficient resolution for boundary layer development and wake interaction.

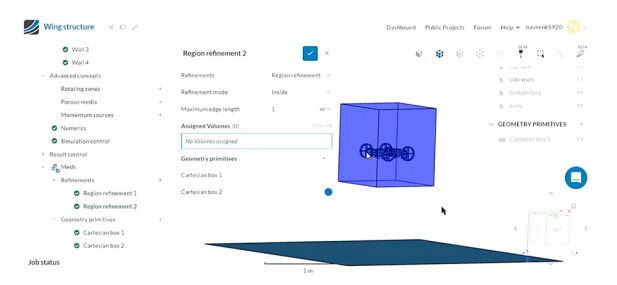


Figure 8: CFD domain setup in SimScale with refined mesh regions enclosing the UAV to capture detailed boundary layer behavior and wake dynamics under 15 m/s inlet flow.

Viscous forces along the X-axis peaked at ~0.6 N, reflecting aerodynamic drag opposing forward motion, before stabilising in steady flow. Lateral and vertical viscous forces were negligible, supporting directional stability. Pressure moments were strongest about the Y-axis (~1.2 N·m), indicating possible yaw imbalance from asymmetric flow near the EDF ducts, while X and Z-axis moments remained negligible, confirming pitch—roll stability. Porous moment analysis showed consistent Z-axis resistance (~2 units), highlighting the need for yaw compensation. Pressure forces were dominated by a thrust-aligned X-axis component (~5 units), with minimal fluctuations elsewhere.

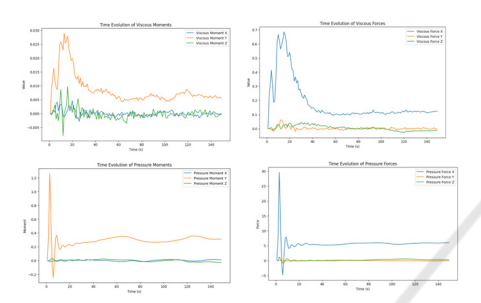


Figure 9: Time evolution plots of viscous and pressure forces and moments from CFD simulation.

#### 4 ALIVE DETECTION SYSTEM

In the domain of Urban Search and Rescue (USAR), the ability to identify the presence and status of human victims in obstructed or hazardous environments remains a critical challenge. Past approaches, as detailed in studies such as Ingle & Chunekar (Ingle & Chunekar, 2016) and Kalaboina et al. (Kalaboina et al., 2018), have relied on ultrasonic, PIR, and low-resolution camera systems for motion and heat-based human detection.

Traditional sensing methods struggle with static or unconscious individuals and are prone to environmental noise. To overcome this, we implemented a computer vision-based alive detection pipeline, simulated on a MacBook Air using its webcam. The system integrates three modules: (i) YOLOv8 for person detection, (ii) MediaPipe FaceMesh to assess consciousness via Eye Aspect Ratio (EAR), and (iii) Farneback optical flow to detect breathing through pixel-level thoracic motion over a temporal buffer. Each subject is classified as Alive and Conscious (eyes open, breathing), Alive and Unconscious (eyes closed, breathing), Dead (no motion or eye activity), or Obstructed/Not Visible. Outputs include timestamped detection logs, GPS

coordinates (simulated), and status saved in JSON format for integration with geo-tagged rescue interfaces.



Figure 10: Output states from the simulated alive detection system showing classification into "Alive & Conscious", "Alive but Unconscious", and "Dead" based on eye and breathing activity.

We propose embedding the detection pipeline into the wall-climbing UAV using Intel RealSense D435i (depth/obstacle detection), RealSense T265 (pose estimation), and an MTF-01P optical flow sensor, managed through a Raspberry Pi running ROS. The alive\_detector.py node will publish real-time human status, confidence, and obstruction flags, with depth discontinuity aiding occlusion detection when YOLO fails.

## 5 CONTROL SYSTEM

Model Predictive Control (MPC) governs the UAV's behaviour across three stages: sticking, tilting, and thrust-based climbing. In the sticking phase, MPC controls wheel torque to ensure zero wall-plane velocity. During tilting, it regulates EDF gear rotation for smooth, constrained motion. In the thrust phase, MPC coordinates EDF thrust and wheel torque to stabilise climbing while maintaining roll, pitch, and tilt limits. The UAV model, built using URDF/Xacro, includes structural and inertial details, focusing on EDF and tilt joints. The MPC state vector includes position, velocity, orientation, tilt angle, and thrust, with inputs as thrust vectors and torques. Stagespecific cost functions and constraints (e.g., torque bounds, joint limits) ensure energy-efficient, stable tracking.

For perception, the UAV uses an Intel RealSense camera indoors to capture RGB-depth data for alive detection via optical flow and pose estimation through odometry. Outdoors, GPS is used for

mapping victim locations, enabling robust operation across environments. To validate the control framework, initial testing was conducted on a standard quadcopter using PX4's MPC Multirotor Rate Model with body rate and thrust inputs. A figure-eight reference trajectory was tracked at constant altitude by discretizing parametric equations, confirming smooth, accurate tracking thus establishing a baseline for extending MPC control to the more complex tilt-rotor UAV platform.

$$x(t) = r cos(\omega t)$$

$$y(t) = r sin(2\omega t)$$

$$z(t) = z0$$

/Anne\_wn/Target-Tracker/pre/upst-offbased\_wn/install/psd\_mpc/phare/psd\_mpc/cosfig-rid\*-RVIz  $= 10$  ×

| Memory wn/Target-Tracker/pre/upst-offbased\_wn/install/psd\_mpc/phare/psd\_mpc/cosfig-rid\*-RVIz  $= 10$  ×

| Memory wn/Target-Tracker/pre/upst-offbased\_wn/install/psd\_mpc/phare/psd\_mpc/psd\_

Figure 11: MPC-based quadcopter simulation in RViz showing tracking of a figure-eight trajectory.

To ensure real-time tracking, the reference trajectory was interpolated between sampled waypoints so the MPC solver always received a continuous setpoint. At each timestep, the control loop retrieved the UAV's state, computed tracking error, constructed the MPC state vector and reference horizon, and solved for optimal control inputs, which were published as VehicleRatesSetpoint messages. Visualisation in RViz was achieved using helper functions that converted predicted state vectors into PoseStamped messages and markers for intuitive path comparison. Simulations demonstrated that the quadcopter successfully tracked a figure-eight path with smooth transitions and minimal deviation, validating the MPC design. The green curve (reference), red marker (current setpoint), and blue path (predicted trajectory) in RViz confirmed effective error minimisation and stability.

The MPC cost function minimized the error between the predicted state and the figure-eight reference while penalizing control effort:

$$\min_{u_{0:N-1}} \sum_{k=0}^{N} |x_k - x_k^{\text{ref}}|_Q^2 + |u_k|_R^2$$

## 6 CONCLUSION

The design and simulation of a wall-climbing UAV specifically suited for search and rescue missions in dangerous, fire-prone areas are presented in this paper. The UAV's servo-driven tilt-rotor mechanism, which has been verified by structural and aerodynamic analyses with SimScale, allows it to transition between flight and vertical surface adhesion. Strength, maneuverability, and thermal resilience are guaranteed by essential elements like high-thrust EDFs, PLA frames, and carbon fiber reinforcements. Real-time sensors, a ROS-based compute unit, and a specially designed alive detection pipeline that can recognize human life signs using YOLOv8, MediaPipe eye tracking, and optical flowbased breathing detection are all integrated into the UAV's electronics.

The detection system, successfully simulated on a laptop, classifies individuals into four states: Alive & Conscious, Alive but Unconscious, Dead, and Obstructed. It logs results with GPS metadata for mapping and rescue coordination. Future work will involve full hardware integration, real-time testing with ROS nodes, and validation of control strategies through Model Predictive Control (MPC) in Gazebo. The UAV will be fire-hardened using Nomex insulation and tested in indoor and outdoor scenarios to enable autonomous operation in real-world disaster environments.

## 7 FUTURE WORK

In the next phase, we will focus on physical prototyping and validation. A fully integrated UAV will be fabricated using a PLA frame coated with Nomex to improve fire resistance, with thermal resilience assessed through heat flux and flame exposure simulations. Indoor and outdoor trials will evaluate surface stability, wall-climbing performance, and autonomous navigation under challenging conditions, including strong ambient light where Intel RealSense sensors may underperform. Real-time alive-detection inference will be optimised on Raspberry Pi or NVIDIA Jetson

modules, with endurance testing incorporating power consumption measurements. Limitations in EDF efficiency and flight time will be addressed through revised propulsion strategies and adaptive energy management.

#### REFERENCES

- Akhloufi, T., et al. (2020). Optical flow-based motion analysis for search and rescue. Computer Vision and Image Understanding, 190, 102–118. https://doi.org/10.1016/j.cviu.2019.102847
- Dudek, J., & Jenkin, M. (2010). Computational principles of mobile robotics. Cambridge University Press.
- Ingle, P., & Chunekar, R. (2016). Human detection in disaster zones using PIR and ultrasonic sensors. International Journal of Advanced Research in Electronics and Communication Engineering, 5(7), 1201–1205.
- Joseph, L. (2018). Learning robotics using Python (2nd ed.). Packt Publishing.
- Kalaboina, K., Mandala, S., & Kumar, M. S. V. (2018). Smart human detection robot using PIR and ultrasonic sensors. International Journal of Engineering Research & Technology, 6(13), 141–145.
- Kim, S., et al. (2018). Biologically inspired wall-climbing robots. Annual Review of Control, Robotics, and Autonomous Systems, 1, 365–391. https://doi.org/ 10.1146/annurev-control-060117-105058
- Lee, Y., et al. (2020). Fireproofing of UAV airframes using ceramic insulation. Journal of Intelligent & Robotic Systems, 97(2), 123–134. https://doi.org/10.1007/s10846-019-01076-7
- Li, C., et al. (2017). Gecko-inspired climbing UAVs with adhesive microstructures. Bioinspiration & Biomimetics, 12(4). https://doi.org/10.1088/1748-319 0/aa7e59
- Li, Y., Gao, J., & Zhang, H. (2021). AI-driven UAV reconnaissance for post-disaster damage assessment. IEEE Transactions on Humanitarian Technology, 9(3), 145–152. https://doi.org/10.1109/THT.2021.3076548
- Mishra, N. (n.d.). Emergency response and search and rescue. Retrieved from https://www.nikhileshmishra.com/emergency-response-and-search-and-rescue/
- Mulgaonkar, C., et al. (2016). Power and weight optimization for micro aerial vehicles. IEEE Robotics & Automation Magazine, 23(4), 78–89. https://doi.org/10.1109/MRA.2016.2601932
- Murphy, R. (2004). Trial by fire: Lessons from rescue robotics. IEEE Robotics & Automation Magazine, 11(3), 50–61. https://doi.org/10.1109/MRA.2004.1337848
- Myeong, H., & Myung, H. (2020). A bio-inspired quadrotor with tiltable rotors for improved wall-perching and climbing. IEEE/ASME Transactions on Mechatronics, 25(4), 1809–1819. https://doi.org/10.1109/TMECH. 2020.2969117

- Patel, A., Deshmukh, R., & Srinivasan, M. (2020). Deep learning-enabled UAVs for victim detection in disaster zones. In International Conference on Intelligent Systems (pp. 231–238). IEEE.
- Redmon, J., et al. (2018). YOLOv3: An incremental improvement. arXiv:1804.02767. https://arxiv.org/abs/1804.02767
- Siegwart, R., Nourbakhsh, I. R., & Scaramuzza, D. (2011). Introduction to autonomous mobile robots (2nd ed.). MIT Press.
- Sharma, A., & Mahapatra, A. (2021). Breath detection in disaster victims using vision-based optical flow. Procedia Computer Science, 186, 89–96. https://doi.org/10.1016/j.procs.2021.04.103
- Spenko, M., et al. (2012). Electroadhesion technology for robotic perching. IEEE Transactions on Robotics, 28(5), 1079–1089. https://doi.org/10.1109/TRO.2012. 2208773
- Sun, L., et al. (2021). Quadcopters with active suction mechanisms for wall traversal. IEEE Access, 9, 11341– 11352. https://doi.org/10.1109/ACCESS.2021.3050234
- Tan, R., et al. (2021). Thermal survivability of UAVs in industrial fires. Sensors, 21(18), 1–14. https://doi.org/10.3390/s21186102
- TheTechArtist. (n.d.). Robots for hazardous environments.

  Retrieved from https://thetechartist.com/robots-for-hazardous-environments/
- Wang, H., et al. (2021). Magnetic wall-climbing drones for structural inspection. Automation in Construction, 133, 103–122. https://doi.org/10.1016/j.autcon.2021.103982
- Zhang, F., et al. (2020). MediaPipe face mesh: A real-time face landmark system. Google AI Blog. https://ai.googleblog.com/2020/08/mediapipe-facemesh.html
- Zhang, W., et al. (2021). Fire-resistant UAV design with silica-based aerogels. Materials Today: Proceedings, 36, 82–88. https://doi.org/10.1016/j.matpr.2020.04.373